PARAMETRIC STUDY OF A NOVEL GRAVITY ASSISTED LOOP HEAT PIPE (GALHP) WITH COMPOSITE MESH-SCREEN WICK STRUCTURE

Xingxing Zhang[1]*, Peng Xu[2], Jingchun Shen[1], Llewellyn Tang[1]*, Di Hu[1], Manxuan Xiao[1], Yupeng Wu[3]
*Author for correspondence
[1] Department of Architecture and Built Environment, University of Nottingham Ningbo China
[2] School of Environment and Energy Engineering, Beijing University of Civil Engineering and Architecture, China
[3] Department of Architecture and Built Environment, University of Nottingham, UK
* Corresponding author: Xingxing.Zhang@nottingham.edu.cn; Llewellyn.Tang@nottingham.edu.cn

ABSTRACT

This article carried out a parametric study of the thermal performance of a novel gravity assisted loop heat pipe (GALHP) with composite mesh-screen wick structure. A refined three-way structure with interior liquid-vapour separator was developed on top of the evaporator to enable a gravity-assisted operation, which not only simplified the corresponding wick structure but also eliminated the 'dry-out' potential in conventional GALHPs. A dedicated simulation model was developed on basis of the heat transfer and the flow characteristics derived from the governing equations of mass, energy, and momentum. This model has been validated by authors' experiment work with the ability to predict the GALHP thermal performance at a reasonable accuracy. It was found that the GALHP thermal performance, represented by the reciprocal of overall thermal resistance, varies directly with applied heat load, evaporator diameter, vapour-liquid separator diameter, and mass flow rate of cooling fluid in the jacket, but inversely with condensation temperature. The research results will be useful for further design, optimisation, and application of such GALHP in the gravity-assisted circumstance.

INTRODUCTION

Loop heat pipe (LHP) is an advanced heat transfer device that circulates the working fluid in a closed loop arrangement by the capillary force developed in a fine pore wick structure. The distinct physical feature of a LHP over to a conventional heat pipe is the separated vapour and liquid transportation lines, leading to less flow entrainment and pressure loss. Such particular configuration of LHP makes it capable to transport large heat flux in long distance.

In 1970s, the first LHP was developed and tested for application in the aerospace by Maydanik et al., [1]. Thereafter, extensive analyses of LHP have been carried out in component designs, mathematical models and optimum wick structures, all of which aimed to achieve the high overall heat transfer coefficient. As a reliable thermal mechanism, LHP has been developed in different configurations and types for various applications which are widely applied in the thermal controls of satellites/spacecraft, electronics and heat-recovery systems. Riehl and Dutra [2] described an experiment LHP to accomplish the thermal management for space mission of up to 70 W by using acetone as the working fluid. Vladimir et al., [3] proposed a low-noise cooling system for computers on the base of LHPs with the heat dissipation up to 180W and the thermal resistance of 0.29°C/W. Li et al., [4] carried out the experimental study on a copper–water LHP with dual parallel condensers for high power light-emitting diode (LED) illumination applications, whose results showed the LHP has a total thermal resistance ranging from 1.0 to 0.4 °C/W with heating loads ranging from 30 W to 300 W.

NOMENCLATURE

A	area, m^2	ρ	density, kg/m^3
c_p	specific heat capacity, J/kg °C	ε	porosity of the wick
D	diameter, m	***Subscripts***	
g	gravity acceleration, m/s^2	*0*	external layer
h	heat transfer coefficient, $W/(m^2\,°C)$	*1*	layer 1
h_{fg}	latent heat of vaporization, J/kg	*2*	layer 2
H	height, m	*3*	layer 3
k	thermal conductivity, W/(m °C)	*cf*	cooling fluid
K	wick permeability, m^2	*cond*	condenser
L	length, m	*eff*	effective
$\dot{m}$	mass flow rate, kg/s	*eva*	evaporator
p	pressure, pa	*g*	gravity
ΔP	pressure drop (pa)	*GALHP*	Gravity LHP
q	heat load per unit area, W/m^2	*hp*	heat pipe
$\dot{Q}$	applied heat load, W	*i*	inner; point i
Pr	Prandtl number	*int*	interface
r	radius, m	*l*	liquid
R	thermal resistance, °C/W	*ll*	liquid line
R_v	vapour constant, kJ/(kg °C)	*lf*	liquid film
Re	Reynolds number	*o*	outer
T	temperature, °C	*tl*	transporting line
u	velocity, m/s	*tw*	three-way structure
Greek		*v*	vapour
μ	dynamic viscosity, kg/(m s)	vl	vapour line

In recent years, application of the LHPs in solar thermal field has become attractive with the significant development of renewable energy [5], where the LHPs normally work in the gravity-assisted conditions, regarding as the GALHP. However, the conventional GALHPs usually have two shortfalls: (1) high-cost and complex evaporator/wick structures; (2) 'dry-out' potential of the liquid film on upper-side wick structure in the evaporator, which is mainly because the insufficient wick capillary force can only elevate the liquid film to a limited height. As a result, a novel GALHP with the top-positioned vapour-liquid separator is developed in this article to not only simplify the wick structure but also eliminate the 'dry-out' potential, enabling a high-efficient and cost-effective GALHP solution. An experimental evaluation and parametric analysis of several impact factors of such innovative GALHP will be

implemented based on the authors' previous work [6]. The research results are expected to provide some clues for further design, optimisation, and application of this GALHP in the gravity-assisted heat-transfer conditions.

LHP DESIGN AND THEORETICAL MODEL

Schematic design of the GALHP vapour-liquid separator is illustrated in Figure 1 (a), which is positioned on top of the evaporator with internally separated vapour and liquid flow channels. A piece of '人'-shaped tube with expanded edges was connected to the inner surface of a refined three-way fitting. When compressing its bottom expander edge against the wick structure tightly, the returned liquid will be evenly distributed from the evaporator top across the wick surface owing to the equivalent gravity/capillary force within the wick structure. Due to such innovative design, the evaporated fluid could be delivered upwards through the vapour line to the condenser in the cooling jacket while the condensed liquid could return dowwards through the liquid line into the evaporator from the top, enabling the entire wick saturated. This design not only creates the clear vapour/liquid flow transportation lines, but also presents a feasible solution to the 'dry-out' potential that exists in conventional GALHPs. Figure 1 (b) shows the detailed dimentions of the developed GALHP while other technical data of the loop components are given in Table 1.

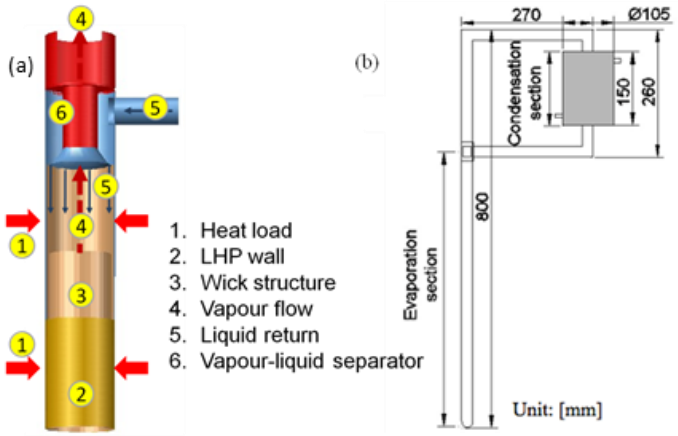

Figure 1 (a) vapour-liquid separator of GALHP and (b) dimensions of developed GALHP

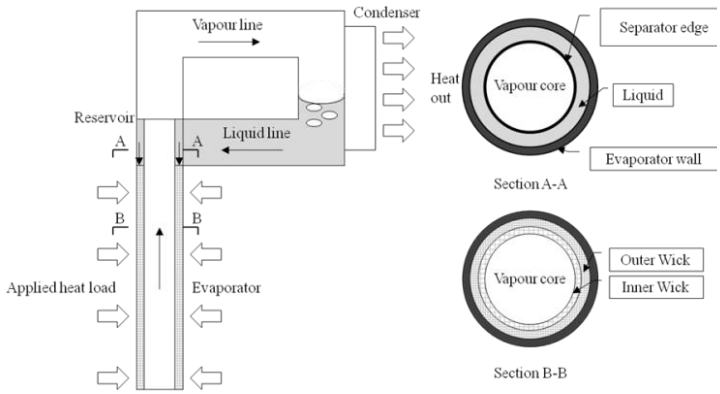

Figure 2 Schematic of the proposed LHP and cross sections of the evaporators

Table 1: Design parameters of the GALHP operation

Parameters	Value	Unit
External diameter of heat pipe	0.022	m
Internal diameter of heat pipe	0.0196	m
Internal diameter of liquid-vapour seporator	0.014	m
Thermal conductivity of evaporator wall	394	W/(m ºC)
Vacuum level	1.3×10^{-4}	Pa
Evaporator length	0.540	m
Length of vapour line	0.585	m
Length of liquid line	0.475	m
Evaporator-to-condenser height difference	0.26	m
Liquid filling level	60	ml
Heat pipe transportation line length	1.0/0.9	m
Wire diameter (wick layer I)	7.175×10^{-5}	m
Layer thickness (wick layer I)	3.75×10^{-4}	m
Mesh number (wick layer I)	6299	/m
Wire diameter (wick layer II)	12.23×10^{-5}	m
Layer thickness (wick layer II)	3.75×10^{-4}	m
Mesh number (wick layer II)	2362	/m
Diameter of cooling jacket	0.1	m
Length of cooling jacket	0.15	m
Conductivity of of cooling jacket wall	16.28	W/(m ºC)

During the steady-state conditions, when a certain amount of heat load is applied to the GALHP evaporator, most of the heat is transferred to the condenser through the phase-changing process, and the rest heat is represented as the thermal loss. The overall operation is maintained as long as the heat load is applied. A schematic view of the proposed GALHP is shown in Figure. 2. The dedicated mathematical model and the associated computer program has been developed to analyse the characteristics of the new GALHP. The mathematical model for this process is based on the following assumptions: 1) Heat transfer and fluid flow are under the quasi-steady state condition; 2) Heat conduction and fluid flow across the wick is one-dimensional in the radial direction; 3) Heat-pipe evaporator is heated axial-symmetrically and the difference of the temperature along the axial direction is negligible; 4) The hydrostatic pressure drop across the radial direction owing to the gravity effect is considered to be zero; 5) The axial pressure drop is negligible due to less magnitude against the gravitational head; 6) The working fluid is incompressible and has the constant property value on each phase; 7) The wick is liquid saturated and wick material is assumed homogenous and isotropic; 8) A local thermal equilibrium is existed between the porous structure and the working fluid; 9) Heat loss to the surroundings is ignored due to the well-insulated pipes. With these assumptions, the fundamental governing equations for vapour and liquid phases (mass continuity, energy and Darcy law) are as follows [7, 8]

$$\nabla \cdot u = 0 \qquad [1]$$

$$\nabla \cdot \dot{q} = k\nabla^2 (T) \qquad [2]$$

$$u = -\frac{K}{\mu}\nabla p \qquad [3]$$

The mass flow rate within the wick structure is considered the constant owing to the mass conservation law, expressed by

$$\dot{m} = \rho_l u_l 2\pi r L_{eva} \varepsilon_w = \frac{\dot{Q}}{h_{fg}} \qquad [4]$$

As the evaporator is heated symmetrically along the axial direction, the analysis of energy conservation and temperature profile in the evaporator will focus on the radial cross-section of the wick structure. The energy conservation equations of the single wick structure are given by [8, 9]

$$\frac{\partial^2 T_w}{\partial r^2} + \frac{1}{r}(1-\alpha)\frac{\partial T_w}{\partial r} = 0 \qquad [5]$$

And the boundary conditions are

$$\begin{cases} T(r)\big|_{r=r_{w,o}} = T_{w,o} \\ T(r)\big|_{r=r_{w,i}} = T_{w,i} \end{cases} \qquad [6]$$

As a result, the overall thermal conductance of the composite wick structure can be given by

$$G_w = \frac{k_{eff,i}A_{w,3}}{(T_{w,1}-T_{w,3})} \times \frac{\partial T_w}{\partial r}\bigg|_{r=r_{w,3}} = \frac{(T_{w,2}-T_{w,3})}{(T_{w,1}-T_{w,3})} \times \frac{k_{eff,i}A_{w,3}}{(T_{w,2}-T_{w,3})} \times \frac{\partial T_w}{\partial r}\bigg|_{r=r_{w,3}} = \frac{(T_{w,2}-T_{w,3})}{(T_{w,1}-T_{w,3})} \times G_{w,i} \qquad [7]$$

The pressure drop of working fluid passing through the porous wick structure is described according to the Darcy's law [7, 8]

$$\frac{\dot{m}\mu_l}{\rho_l K_w} = -2\pi r L_{eva}\frac{\partial P_w}{\partial r} \qquad [8]$$

The pressure distributions in this composite wick structure are

$$\begin{cases} r_3 \le r \le r_2, P_w(r) = P_v - \frac{\dot{m}\mu_l}{2\pi\rho_l K_{w,o} L_{eva}}\ln(r_2/r_1) - \frac{\dot{m}\mu_l}{2\pi\rho_l K_{w,i} L_{eva}}\ln(r/r_2) \\ r_2 \le r \le r_1, P_w(r) = P_v - \frac{\dot{m}\mu_l}{2\pi\rho_l K_{w,o} L_{eva}}\ln(r/r_1) \end{cases} \qquad [9]$$

The total pressure drop after passing through the saturated wick structures are

$$\Delta P_w = -\left[\frac{\dot{m}\mu_l}{2\pi\rho_l K_{w,o} L_{eva}}\ln(r_2/r_1) + \frac{\dot{m}\mu_l}{2\pi\rho_l K_{w,i} L_{eva}}\ln(r_3/r_2)\right] \qquad [10]$$

In a heat pipe operation, the maximum capillary pumping head ($\Delta P_{c,max}$) must be greater than or at least equal to the total pressure drops along the heat pipe. In this particular design, as the heat pipe works at a gravity-assisted condition, the gravitational head (ΔP_g) becomes positive. The pressure relationship is hereby characterized as

$$\begin{cases} \Delta P_{c,\max} + \Delta P_g \ge \Delta P \\ \Delta P = \Delta P_{eva} + \Delta P_{tw} + \Delta P_{vl} + \Delta P_{cond} + \Delta P_{ll} + \Delta P_w \end{cases} \qquad [11]$$

The total pressure drops in the condenser includes the vapour and liquid pressures drops

$$\Delta P_{cond} = \Delta P_{cond,v} + \Delta P_{cond,l} \qquad [12]$$

The vapour pressure drop in the condenser section can be written as

$$\Delta P_{cond,v} = F_{cond,v}\left(\frac{H_{cond}}{2}\right)\dot{Q} \qquad [13]$$

where, $F_{cond,v}$ is the vapour frictional coefficient in the heat exchanger, The liquid pressure drop is described

$$\Delta P_{cond,l} = F_{cond,l}\left(\frac{H_{cond}}{2}\right)\dot{Q} \qquad [14]$$

where, $F_{cond,l}$ is the liquid frictional coefficient in the condenser, defined as

$$F_{cond,l} = \frac{4\mu_l}{\pi(D_{cond}{}^2 - D_{lf}{}^2)\rho_l h_{fg}} \qquad [15]$$

The liquid pressure drop in the liquid transportation line is

$$\Delta P_{ll} = F_{ll} L_{ll} \dot{Q} \qquad [16]$$

where, F_{ll} is the liquid frictional coefficient in the liquid transportation line, defined as

$$F_{ll} = \frac{4\mu_l}{\pi D_{ll}{}^2 \rho_l h_{fg}} \qquad [17]$$

The overall thermal resistance of the GALHP is defined as

$$R_{GALHP} = R_{eva} + R_p + R_{lf} + R_{cond,wall} + 1/h_{cf} \qquad [18]$$

Inside, the thermal resistance from the evaporator wall to the inner surface of composite wick structure in GALHP evaporator is expressed as

$$R_{eva} = \frac{T_{eva,wall} - T_v}{\dot{Q}} \qquad [19]$$

The thermal resistance due to pressure drop in the GALHP is

$$R_p = \frac{(T_v + 273)^2 R_0 \Delta P}{\dot{Q} h_{fg} P_v} \qquad [20]$$

The condensed liquid film is assumed evenly distributed on the surface of condenser and its associated flow resistance is

$$R_{lf} = \frac{\ln\left[D_{cond,i}/(D_{cond,i} - 2\delta_{lf})\right]}{2\pi L_{lf} k_{lf}} \qquad [21]$$

The thermal resistance of GALHP wall in the condenser is

$$R_{cond,wall} = \frac{\ln(D_{cond,o}/D_{cond,in})}{2\pi L_{cond} k_{cond}} \qquad [22]$$

The heat transfer coefficient of cooling fluid in the jacket is

$$h_{cf} = C\,\mathrm{Re}_{cf}{}^n\,\mathrm{Pr}_{cf}{}^{1/3} \qquad [23]$$

RESULTS OF PARAMETRIC STUDY

It needs to be addressed that the developed theoretical model has been validated by authors' previous experiment work with the ability to predict the GALHP thermal performance at a reasonable accuracy.

Temperature and pressure-drop profiles in the wick structure

Temperature and pressure-drop profiles along the radius direction in the wick structure under different applied heat load were displayed in Figure 3. The temperature was relatively lower at the smaller radius (close to internal wick surface) than that at the larger radius (close to external wick surface), e.g., the temperature increased from 38.24 to 40.42^{o}C under the 100W heat load whilst varying from evaporator radius from 9.0 to 9.8mm. However, the pressure drop varied oppositely with the radius, which was nearly zero at the point close to the external wick surface and increased towards the internal wick surface, e.g., the pressure drop decreased from 0.015×10^{-3} to 0.000039×10^{-3} Pa under the 100W heat load whilst varying from evaporator radius from 9.0 to 9.8mm. In addition, the sharp variations of pressure drops in the external wick layer were also observed owing its larger flow resistance than the internal wick layer. But the temperature variation didn't show too much difference in these two wick layers mainly due to the small magnitudes of the pressure drops, whose impact on the ultimate temperature were very limited. Both the temperature and the pressure drop decreased more under the higher applied heat load, e.g., 2.60^{o}C/0.021×10^{-3} Pa of temperature/pressure drops at 120W heat load but only 0.44^{o}C/0.00057×10^{-3} Pa of temperature/pressure drops at 20W heat load. This is because the larger applied heat load enhanced the thermodynamic activities of the working fluid, resulting in the corresponding higher temperature and pressure drops. In overall, it was concluded the pressure drops in such compound mesh-screen wick structure could be ignored in future design and optimization due to their very small magnitudes.

Impact of evaporator diameter

Impact of the evaporator diameter on the GALHP thermal performance under different applied heat load levels was investigated using the verified simulation model by varying the evaporator diameter from 10 to 24mm while remaining rest design and operation parameters the same, i.e., 30^{o}C of condensation temperature, 14mm of separator diameter, and l l/min of cooling-fluid flow. It was seen from Figure 4 that the GALHP with larger evaporator diameter had the lower evaporator temperature and the lower overall thermal resistance, benefiting from the enhanced heat-transfer ability with less flow resistance/pressure drops inside the evaporator. Both the evaporator temperature and the overall thermal resistance decreased obviously when the evaporator diameter was less than 20mm but reduced slightly when the evaporator diameter was over 20mm. When increasing the applied heat load, it led to higher temperatures of the working fluid and the evaporator. However, the different heat load had the very limited reducing effect on the overall thermal resistance whenever the evaporator changed. The heat-transfer limits were respectively achieved by the GALHP when the evaporator diameter was at 18mm under heat load of 20W and 10mm under heat load of 40W. As a result, the evaporator diameter of such GALHP was recommended at more than 20mm.

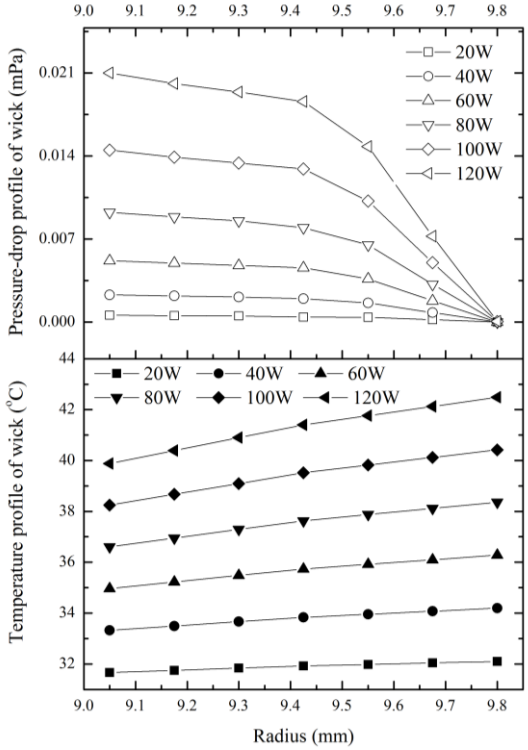

Figure 3 Temperature and pressure-drop profiles along the radius direction in the wick structure

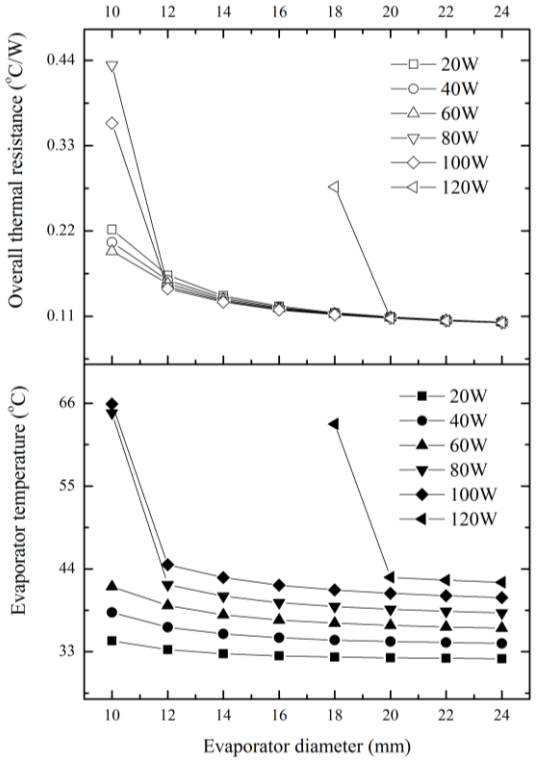

Figure 4 Impact of evaporator diameter on the GALHP thermal performance

Impact of separator diameter

Varying the separator diameter from 4 to 18mm while leaving the rest design and operation parameters unchanged, i.e., 22mm of evaporator diameter, 30°C of condensation temperature, and l l/min of cooling-fluid flow, impact of the separator diameter on the GALHP thermal performance under different applied heat load levels was carried out using the verified simulation model as shown in Figure 5. Similar as the impact of evaporator diameter, the larger separator diameter led to the reductions of both evaporator temperature and overall thermal resistance, owing to the enhanced heat-transfer ability with less flow resistance/pressure drops inside the separator. Both the evaporator temperature and the overall thermal resistance decreased a lot when the separator diameter was less than 10mm but reduced slightly afterwards. Higher applied heat load raised temperatures of both the working fluid and the evaporator. However, the levels of heat load had the very limited reducing impact on the overall thermal resistance whenever the separator changed. The heat-transfer limits were respectively achieved by the GALHP when the separator diameter was at 10mm under heat load of 20W and 6mm under heat load of 40W. It was therefore recommended that the separator diameter of such GALHP should be more than 10mm.

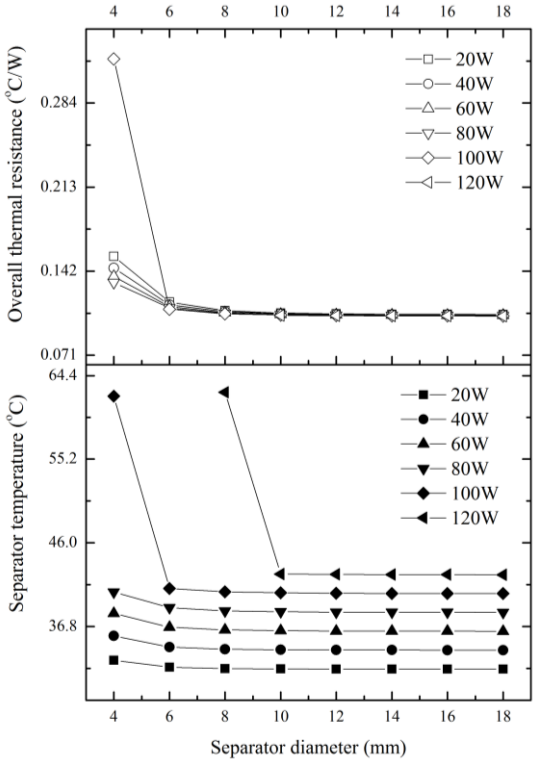

Figure 5 Impact of separator diameter

Impact of condensation temperature

Varying the condensation temperature from 5 to 45°C while remaining other design and operation parameters the constant, i.e., 22mm of evaporator temperature, 14mm of separator diameter, and l l/min of cooling-fluid flow, impact of the condensation temperature on the GALHP thermal performance under different applied heat load levels was presented in Figure 6 using the verified simulation model. Higher condensation temperature corresponded to higher temperature of working fluid inside the GALHP and therefore led to higher evaporator temperature, whose variation showed as a liner relationship. On the other hand, an upwards-opening parabolic relationship was found in between the condensation temperature and the overall thermal resistance of this GALHP. Increasing the condensation temperature initially decreased the overall thermal resistance but then reversed when the condensation temperature was over about 35°C. This phenomenon is because: firstly the thermodynamic attributes of the working fluid was more activated at the higher condensation temperature, which consequently enhanced the heat-transfer ability of working fluid and reduced the overall thermal resistance; but when the condensation temperature increased to a certain level, the temperature difference between the condensation vapour and the cooling fluid was too small, which weakened the heat-transfer process from the GALHP to the cooling fluid in the jacket and accumulated heat inside of the GALHP, leading to the higher thermal resistance. The larger heat load applied to the GALHP increased temperatures of both the working fluid and the evaporator, resulting in the lower overall thermal resistance under the same condensation temperature. It was recommended that the appropriate condensation temperature for this GALHP should be in the region of 20-35°C by considering trade-off between the thermodynamic properties of working fluid and the heat transfer to the cooling fluid in the jacket. In addition, there were no heat-transfer limits occurring in the GALHP during this condensation temperature range.

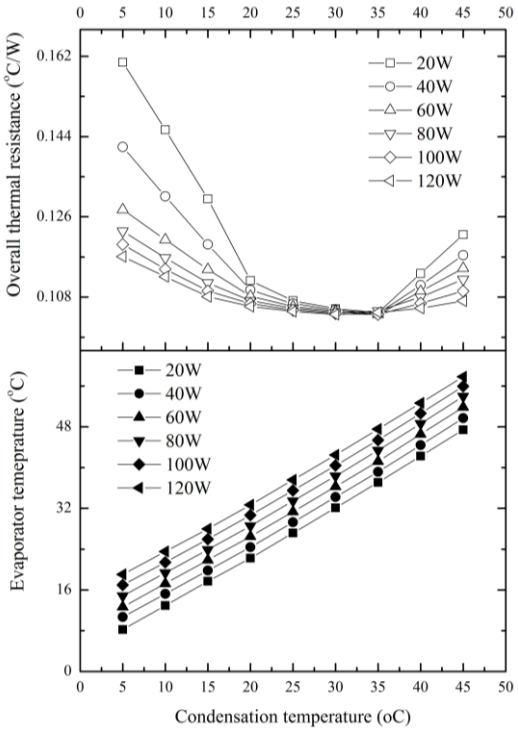

Figure 6 Impact of condensation temperature

Impact of mass flow rate of cooling fluid in the jacket

Varying the mass flow rate of cooling fluid in the jacket from 0.5 to 5 l/min while remaining other design and operation parameters the same, i.e., 22mm of evaporator temperature,

14mm of separator diameter and 30°C of condensation temperature, impact of the mass flow rate of cooling fluid on the GALHP thermal performance under different applied heat load levels was given in Figure 7 using the verified simulation model. It was found that increasing the mass flow rate improved the convective heat transfer coefficient of cooling fluid in the jacket, which thus decreased the evaporator temperature and the overall thermal resistance. Both the evaporator temperature and the overall thermal resistance decreased apparently when the mass flow rate was less than 4.5 l/min but reduced slightly afterwards. However, the impact extent was very limited due to the little enhancement of the convective heat transfer coefficient of cooling fluid, which may require the improved design of the cooling jacket rather than only increasing mass flow rate. The GALHP with larger applied heat load increased temperatures of both the working fluid and the evaporator, and caused lower overall thermal resistance under the same mass flow rate of cooling fluid in the jacket. It was recommended that the appropriate mass flow rate of the cooling fluid in the jacket should be more than 4.5 l/min and an improved design of the jacket for better heat transfer would be also necessary. Besides, there were no heat-transfer limits occurring in the GALHP when the mass flow rate of cooling fluid was over 4.5 l/min.

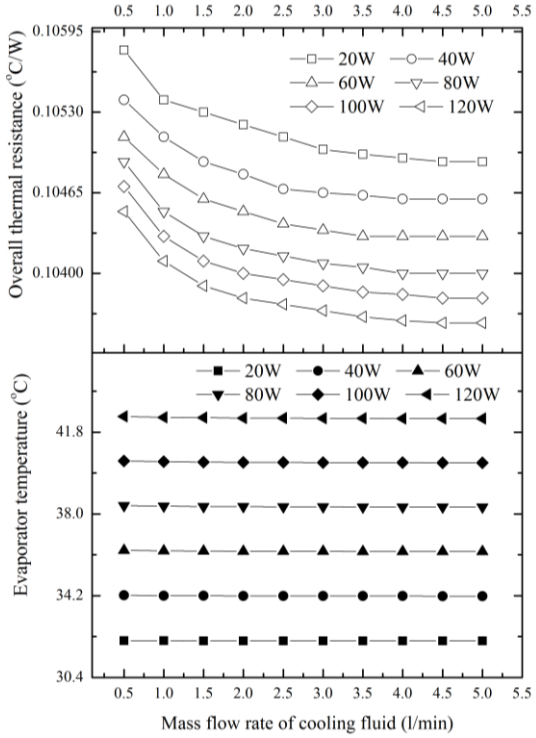

Figure 7 Impact of mass flow rate of cooling fluid

CONCLUSION

A novel GALHP with composite screen wick structure was reported in this article through numerical simulation. A refined three-way structure with interior vapour-liquid separator is developed on top of the evaporator to not only simplify the wick structure but also eliminate the 'dry-out' potential, which is expected to achieve a high-efficient and cost-effective GALHP solution. A dedicated simulation model was developed based to conduct the parametric study. Temperature/pressure profiles in wick structure and several impact factors on GALHP performance were discussed. Appropriate recommendations for further design, optimisation and application of this GALHP in the gravity-assisted heat-transfer conditions were also made as below: (1) pressure drops in the composite screen mesh wick structure could be ignored due to their very small magnitudes; (2) the evaporator diameter should be more than 20mm; (3) the separator diameter is required at more than 10mm; (4) the condensation temperature needs to be in the region of 20-35°C; (5) the mass flow rate of cooling fluid in the jacket should be no less than 4.5 l/min along with an improved thermal design of the jacket itself. The research results will be useful for further design, optimisation, and application of such GALHP in the gravity-assisted circumstance.

ACKNOWLEDGEMENT

The authors would acknowledge sincere appreciation to the financial supports from the Zhejiang Natural Science Foundation (LQ16E060001), the Small research grant of University of Nottingham Ningbo China (2015-2016), the Beijing Key Lab of Heating, Gas Supply, Ventilating and Air Conditioning Engineering, and the BIM-GIS Application in Green Built Environment project, funded by Ningbo Science and Technology Bureau (Grant No. 2015B11011).

REFERENCES

[1]. Y.F. Maidanik, Loop heat pipes, *Applied Thermal Engineering* 25 (2005) 635-657.

[2]. R.R. Riehl, T. Dutra, Development of an experimental loop heat pipe for application in future space missions, *Applied Thermal Engineering* 25 (2005) 101–112.

[3]. Vladimir G. Pastukhov, Yury F. Maydanik, Low-noise cooling system for PC on the base of loop heat pipes, *Applied Thermal Engineering* 27 (2007) 894–901.

[4]. Ji Li et al., A loop-heat-pipe heat sink with parallel condensers for high-power integrated LED chips, *Applied Thermal Engineering* 56 (2013) 18-26.

[5]. X Zhang et al., Socio-economic performance of a novel solar photovoltaic/loop-heat-pipe heat pump water heating system in three different climatic regions, *Applied Energy* 135 (2014) 20–34.

[6]. X Zhang et al., Comparative study of a novel liquid–vapour separator incorporated gravitational loop heat pipe against the conventional gravitational straight and loop heat pipes – Part I: Conceptual development and theoretical analyses, *Energy Conversion and Management* 2015; 90: 409–426.

[7]. T. Kaya, J. Goldak, Numerical analysis of heat and mass transfer in the capillary structure of a loop heat pipe, International Journal of Heat and Mass Transfer 49 (2006) 3211–3220.

[8]. David Reay and Peter Kew, Heat pipes: Theory, Design and Applications, 5th edition, Elsevier, 2006.

[9]. W. Rohsenow, J.Hartnet, Y.Cho, Handbook of Heat Transfer, 3rd edition, McGraw-Hill, 1998.